Target dependence of slow electrons emitted in swift ion-atom collisions

P. D. Fainstein*
Centro Atómico Bariloche, Comisión Nacional de Energía Atómica, Avenida E. Bustillo 9500, 8400 Bariloche, Argentina

R. Moshammer and J. Ullrich
Fakultat für Physik, Universität Freiburg, Hermann-Herder-Strasse 3, 79104 Freiburg, Germany
and Max-Planck-Institut für Kernphysik, 69029 Heidelberg, Germany
(Received 4 December 2000; published 16 May 2001)

Low-energy electron emission is studied for 3.6-MeV/u Au^{53+} impact on Ne and Ar using the first-Born and continuum-distorted-wave eikonal-initial-state (CDW-EIS) approximations. By using optimized effective potentials to represent the target atom, very good agreement is obtained between the CDW-EIS results and experiments. The comparison with the calculations using the first-Born approximation shows that the emission is very asymmetric, with a preferential emission into the forward direction. A detailed study of the emission from each initial orbital of the target atom reveals features in the spectra which can be related to the structure of the initial-state bound wave function.

DOI: 10.1103/PhysRevA.63.062720 PACS number(s): 34.50.Fa, 34.50.Gb, 34.50.−s

I. INTRODUCTION

Electron emission plays a major role in the energy loss of swift ions in different media, and therefore in radiation damage. Depending on the target thickness the impinging ion can suffer single or multiple scattering. However, the basic mechanism by which electrons are produced is that of electron emission in single ion-atom collisions. Of course, the electronic states in solid or biological target differ from those of isolated atoms, but the reaction remains the same. Therefore, it is very important to have a precise knowledge of the electron emission process in ion-atom collisions.

The first measurements of electron emission spectra were performed during the 1960s by Rudd and co-workers [1]. Since then the field has witnessed many major breakthroughs due to the ever increasing precision of experimental techniques, the development of highly charged ion sources, the availability of antiproton beams, etc. At the same time, the theoretical description has evolved from simple first-order theory to the present calculations, which can take into account very accurately a description of target bound and continuum states and the distortion due to the long-range projectile Coulomb potential [2].

Detailed information about the reaction dynamics is provided by doubly differential cross sections (DDCS's) as a function of the electron momenta in the final state. Due to the cylindrical symmetry of the collision with respect to an axis defined by the projectile velocity $\vec{v}$, DDCS's can be expressed either in terms of the electron energy and angle (E_e, θ_e) or the longitudinal and transverse linear momenta $(p_{e\|}, p_{e\perp})$. Two experimental techniques are available to measure DDCS's in ion-atom collisions. In the first the emitted electron energy is measured by an analyzer located at a fixed angle. Varying this angle it is possible to map all the DDCS's [1]. The second method involves the extraction of an emitted electron, by a combination of electric and magnetic fields, which is then recorded by a position-sensitive-detector. This allows one to measure the full momenta of the emitted electron. By simultaneously measuring the recoil ion using a similar technique, and using energy and momentum conservation, it is possible to extract the complete kinematics, i.e., the momentum transfer, the recoil-ion momenta, and the electron spectra, for defined charge states of the residual target [3]. Both methods provide different views of the same spectra of emitted electrons. However, it turns out that both methods are complementary, since they are best suited to different parts of the spectra. The former method has the limitation of measuring low-energy electrons, while the latter is not accurate for high-energy electrons.

At present the final-state electron momentum distribution has been studied mostly in the case of a He target, where the entire momentum space has been explored. These studies were performed with protons up to multiply charged ions. Much less is known about the case of multielectronic targets, where very few experimental and theoretical studies are available. For a target atom with several filled shells, several questions arise which are of great importance, for example, in calculations of radiation damage. Since an electron can be emitted from any shell, it is important to know the relative contributions as a function of projectile charge and velocity. On the other hand, electrons in the initial state fill levels with different values of the principal, angular momentum and magnetic quantum numbers (nlm). One can expect that the final momentum distribution will be different, and will carry information about the corresponding initial state.

In recent experiments using swift highly-charged Au^{53+} ions impinging on He, Ne, and Ar [4,5], it was found that the low-energy part of the electronic momentum distribution depends on the target. These results can be taken as an indirect confirmation of previous theoretical studies, which indicated that there is a target dependence due to the different behavior of the bound and continuum states at the threshold [6]. Therefore it is our purpose to study in more detail the electron emission process close to threshold for different initial

*Electronic address: pablof@cab.cnea.gov.ar

 ©2001 The American Physical Society

states. The study will be performed at a fixed impact energy of 3.6 MeV/amu, which is equivalent to projectile velocity of 12 a.u., for light (H^+) and highly charged ions (Au^{53+}) impinging on Ne and Ar target atoms.

This paper is organized as follows. In Sec. II we present the theoretical models used to obtain the momentum distribution, and discuss the different model potentials used for the calculation of the DDCS's. Section III contains a comparison between the experimental and theoretical results, and a study of the dependence of the DDCS on the initial state. Finally, in Sec. IV we present conclusions. Atomic units will be used.

II. THEORETICAL MODEL

The theoretical description of electron emission in ion-atom collisions requires two basic ingredients. The first is an accurate calculation of the target bound and continuum states. Following the work of Madison [7] within the first-Born approximation, this can be done by assuming that there is only one active electron during the collision. The target can then be replaced by a suitable model potential, and the bound and continuum states have to be calculated numerically.

The second ingredient is to include the distortion in the initial and final channels introduced by the projectile. Due to the long range of the Coulomb potential, two effects appear. The initial bound state is distorted (or polarized), and the final state is aligned, preferentially in the forward direction, due to the attraction of the projectile potential. Theoretically it is very difficult to describe these states of the two-center potential formed by the target and projectile nuclei. A useful method to take these effects into account is distorted-wave theory, which allows one to develop perturbative schemes where the long-range character of the Coulomb potential is taken into account. Many first-order approximations have been conctructed based on this theory. Usually the initial and final distorted wave functions are proposed as

$$\chi_i = \phi_i(\vec{x})\mathcal{L}_i(\vec{s}), \tag{1}$$

$$\chi_f = \phi_f(\vec{x})\mathcal{L}_f(\vec{s}), \tag{2}$$

where $\vec{x}$ ($\vec{s}$) is the coordinate of the active electron in the target (projectile) reference frame, and ϕ_i and ϕ_f the initial bound and final continuum states of the target atom. By choosing different distortions $\mathcal{L}_{if}$, it is possible to define different approximations. One of the most successful is the continuum-distorted-wave-eikonal-initial-state (CDW-EIS) [8,2] model, where the initial target bound state is distorted by an eikonal phase factor ($\mathcal{L}_i$) which takes into account the projectile-electron Coulomb interaction. In the final state, the interaction of the emitted electron with the projectile is introduced through a multiplicative continuum wave function ($\mathcal{L}_f$). Within the CDW-EIS model it is also possible to describe with good accuracy, as in the first-Born approximation, the bound and continuum states of the target [9]. Within the one-active electron approximation the target is represented by a model potential, and the bound and continuum states are obtained numerically by solving the time-independent Schrödinger equation.

Several model potentials are available in the literature, given either in tabular form or by analytical formulas. The most used are the Hartree-Fock-Slater (HFS) potentials of Herman and Skillman [10]. However, these potentials have an incorrect asymptotic behavior which is usually arranged by introducing the so-called Latter correction. Recent research showed that this method can produce unphysical structures in the electron momentum distribution [11]. Therefore it is necessary to use other potentials which do have the correct asymptotic behavior and which provide accurate values of the binding energy and of the bound and continuum wave functions. In the present work we will use those obtained from the optimized effective potential (OEP) method developed by Talman and co-workers [12–14]. The accuracy of these potentials has been tested in comparison with Hartree-Fock calculations, and can be checked in comparison with results obtained from density-functional theory (DFT). The DFT potentials have the correct asymptotic behavior, and, when used within the CDW-EIS model, give results in very good agreement with experiment [11,15]. For example, the binding energy of the $3p$ states of Ar calculated using the OEP is -0.585 a.u. which falls between the values of -0.620 and -0.533 a.u. obtained with the DFT and HFS potentials, respectively. Since the absolute values of the cross sections are closely related to the value of the binding energy, we can expect that the results obtained with the OEP potential will be larger than those from DFT, and smaller than the HFS values. The advantage of OEP potentials over DFT is that they are available for every target in tabular form [13]. Therefore, these potentials will be used in the calculations shown in the following.

III. RESULTS AND DISCUSSIONS

Electrons emitted with very low energy in ion-atom collisions are very difficult to measure. However, the multielectron recoil-ion momentum spectrometer recently developed by Ullrich *et al.* [3] is very well suited for this task. Experiments with this technique achieve unprecedented accuracy at low electron energies, with an electron momentum resolution of $\Delta p_{e\|} = 1 \times 10^{-2}$ a.u. in the longitudinal direction and $\Delta p_{e\perp} = 1.4 \times 10^{-2}$ a.u. in the perpendicular direction. This allows one to measure the so-called soft-collision peak at $E_e = 0$ eV with an accuracy $\Delta E_e = 2.5$ meV. Experiments have been performed using He [4], Ne, and Ar [5] gas targets. In Figs. 1 and 2 the experimental doubly differential cross sections for net ionization of Ne and Ar by 3.6 MeV/u Au^{53+} impact are shown in comparison with theoretical calculation using the first-Born (B1) and CDW-EIS models. For the B1 calculations we have also employed the OEP's. The DDCS's are presented as a function of $p_{e\|}$ for fixed values of $p_{e\perp} = 0.05$, 0.45, and 0.95 a.u. It is clear from the figures that the CDW-EIS results using the OEP are in very good agreement with the experimental data, especially in the case of Ar. Conversely, the results from B1 largely overestimate the experimental results at the peak and for negative values of $p_{e\|}$. A comparison between both models shows that B1 gives a

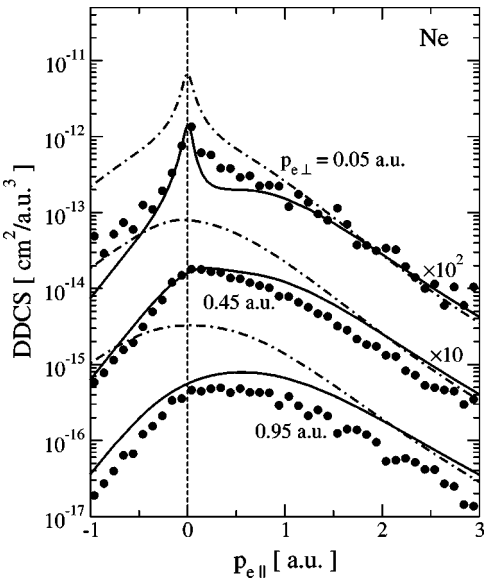

FIG. 1. DDCS for net ionization of Ne by 3.6 MeV/u Au^{53+} impact as a function of $p_{e\parallel}$. Experiments: (●), from Ref. [5]. Theory: solid line, CDW-EIS with the OEP; dot-dashed line, B1 with the OEP.

symmetric peak while the CDW-EIS results are clearly asymmetric in agreement with experiments. Except for $p_{e\perp}=0.05$ a.u., the maximum is shifted to positive values of $p_{e\parallel}$ due to the Coulomb attraction by the highly charged ion. This effect is not present at small values of both $p_{e\parallel}$ and $p_{e\perp}$, due to the large density of states at threshold which produces the peak. In the case of a H target this effect would be even more pronounced, since the density of states diverges at threshold as $1/p_e$, where $p_e^2=p_{e\parallel}^2+p_{e\perp}^2$ is the electron momentum, therefore producing a cusp as the well-known ''electron capture to the continuum'' cusp. In Fig. 2 we also include the CDW-EIS results from Ref. [11] using the DFT potential for Ar. As predicted above from the binding energies of the $3p$ electrons in the initial state, the DFT results are smaller than the present results using the OEP. However, the results from both calculations are very close to each other, showing the same dependence on $p_{e\parallel}$ for the different values of $p_{e\perp}$.

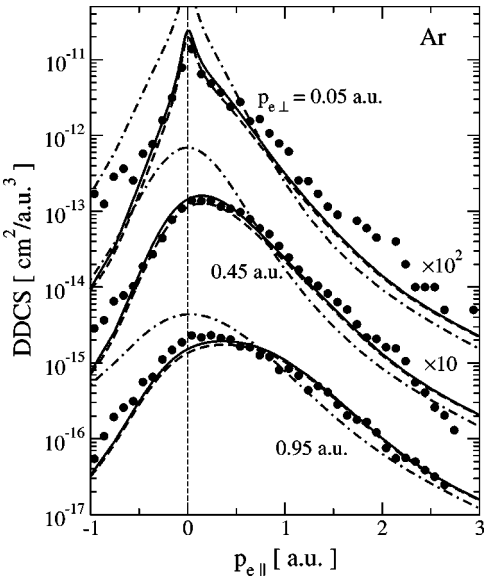

FIG. 2. DDCS for net ionization of Ar by 3.6 MeV/u Au^{53+} impact as a function of $p_{e\parallel}$. Experiments: (●), from Ref. [5]. Theory: solid line, CDW-EIS with the OEP; dot-dashed line, B1 with the OEP; dashed line, CDW-EIS with the DFT potential from Ref. [11].

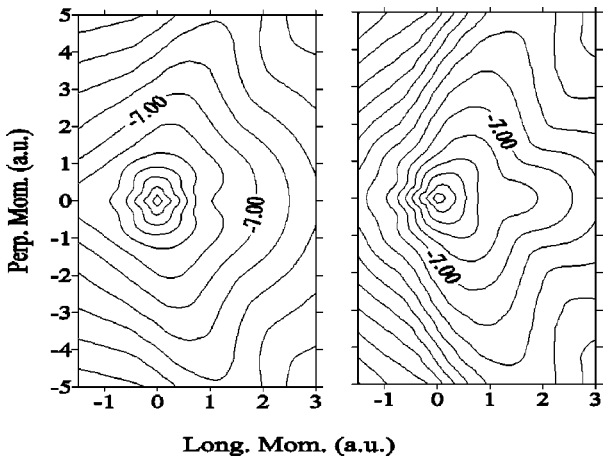

FIG. 3. Contour plot showing the projection onto the $(p_{e\parallel},p_{e\perp})$ plane of the DDCS divided by Z_P^2 for electron emission from the $3s$ state of Ar by 3.6 MeV/u H^+ (left panel) and Au^{53+} (right panel) impact.

More detailed information about the electron emission process can be obtained by studying the contribution from the different initial orbitals of the target. Previous studies [5,11] showed that the main contribution to DDCS's in the momentum range shown in Figs. 1 and 2 come from the outer shells of the target, that is, the $2s$ and $2p$ orbitals of Ne and the $3s$ and $3p$ orbitals of Ar. DDCS's from each initial orbital show a different functional dependence with the longitudinal and transverse momenta. Instead of plotting DDCS's for different cuts, associated with constant values of $p_{e\perp}$, it is more interesting to have a view of the whole distribution in momentum space. A three-dimensional plot of the DDCS as a function of $p_{e\parallel}$ and $p_{e\perp}$ has all the information, but many details are lost since the DDCS varies by several orders of magnitude in a small range of electron momenta. We have therefore chosen to view the results as contour plots which are the projection of the DDCS' onto the $(p_{e\parallel},p_{e\perp})$ plane.

In Figs. 3, 4, and 5, we present the contour plots for 3.6 MeV/amu H^+ and Au^{53+} impact on Ar $3s$, $3p_0$, and $3p_{\pm1}$ initial orbitals. These plots show a striking difference between both projectiles. For H^+ impact the momentum distributions show a preferential emission at 90° ($p_{e\parallel}=0$), which is characteristic of the dipolar transitions that are dominant in the case of light projectiles at high impact energy. As the projectile charge increases, the momentum distribution is shifted in the forward direction due to the Coulomb attraction by the projectile potential. Although the projectile charge is large and the process is nonperturbative (the projectile charge to velocity ratio is 4.4), it is still very surpris-

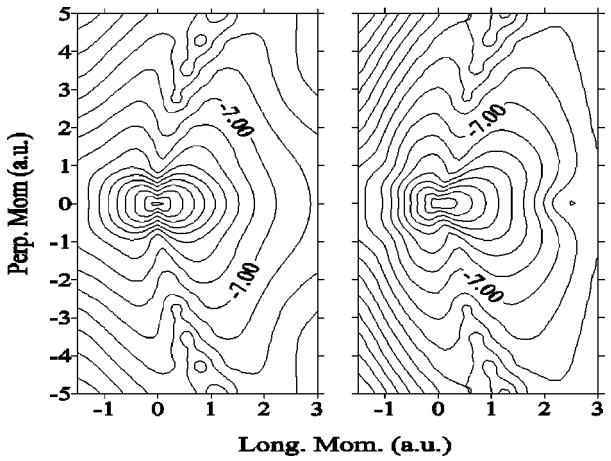

FIG. 4. Same as Fig. 3, but for electron emission from the $3p_0$ state of Ar.

ing that at high velocities the projectile field can produce such a large variation of the momentum distribution at very small electron energies.

A particular feature appears for the $3p_0$ orbital, where there is a pronounced dip close to $p_{e\|}=0$. It can be shown, with a very simplified model, that this feature is related to the nodal structure of the $3p_0$ orbital. Let us consider the first-Born approximation in the limit of $p_e \to 0$. We describe the final continuum state using a hydrogenic wave function with an effective nuclear charge, to be chosen using some recipe which is of no importance here. Therefore the DDCS can be written as

$$\frac{d^2\sigma}{d\vec{p}_e} \approx \frac{4\pi^2 Z_P^2}{v^2} |N(p_e)|^2 \int d\vec{\eta}\, \frac{|\phi_{nlm}(\vec{q}+\vec{p}_e)|^2}{q^2}, \qquad (3)$$

where $\vec{q}$ ($\vec{\eta}$) is the (transverse) momentum transfer by the projectile, Z_P and v are the projectile charge and velocity, ϕ_{nlm} is the initial orbital occupied by the active electron, and $|N(p_e)|$ is the Coulomb density of states, which at threshold behaves as

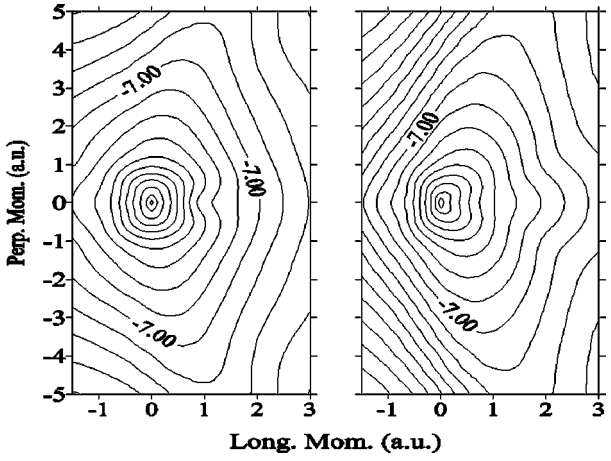

FIG. 5. Same as Fig. 3, but for electron emission from the $3p_{\pm 1}$ state of Ar.

$$|N(p_e)|^2 \approx 1/p_e, \qquad (4)$$

producing the cusp which is characteristic of a pure Coulomb potential. In the present case of multielectronic targets we can suppose that Eq. (3) will remain basically unchanged, except that the density of states given by Eq. (4) will be replaced by a finite density of states associated with the model potential used to describe the target atom (the density of states diverges only for a ''pure'' Coulomb potential). For a given initial orbital defined by the quantum numbers n,l, and m, the integral in Eq. (3) can be solved analytically. Since we are making very crude approximations, it is not necessary to do this; we only need to obtain the most important functional dependence. Solving the integral and taking the limit $p_e \ll v$, it is easy to show that

$$\frac{d^2\sigma}{d\vec{p}_e} \approx |N(p_e)|^2 p_{e\|}^2, \qquad (5)$$

$$\frac{d^2\sigma}{d\vec{p}_e} \approx |N(p_e)|^2, \qquad (6)$$

where Eq. (5) corresponds to initial orbitals with quantum number $l,m=1,0$, and Eq. (6) to $l,m=1,\pm 1$. These results show that the DDCS in the limit of $p_e \to 0$ is given mainly by the density of states at threshold multiplied by a function which depends on the initial state. In the first case the DDCS is proportional to $p_{e\|}$, and thus it is zero when $p_{e\|}=0$. Therefore, the dip shown in Fig. 4 is directly related to the symmetry properties of the initial bound state. The results from B1 differ a little from this simple model, as we can expect more than dipolar contributions, and because the result has a limited range of validity which excludes, for example, the large values of $p_{e\perp}$ where the dip is shifted from $p_{e\|}=0$. This is confirmed by the fact that the shift increases with the projectile charge.

The previous results show that the momentum distribution close to the soft-collision peak is sensitive to the initial state. However, when it is not possible to separate the contribution from each orbital, these signatures are lost. This is shown in Fig. 6, where the contour plots are given, summing the contribution from all the initial states as is given by present day experiments. The distributions now appear as we would expect from our conventional knowledge. For the light projectile close to the peak the emission is symmetrical (note the different scales in both axis) in the longitudinal and perpendicular direction, as one would expect from the major role played by the density of states at threshold as explained above. As the electron momentum increases the emission becomes mainly dipolar, but with contributions from other angular momenta, as is clear from the fact that the emission is not exactly onto $p_{e\|}=0$ but is slightly shifted in the forward direction. When the projectile charge increases the shift is more pronounced, and a change in the distribution is also observed the region near threshold. This is in agreement with previous theoretical results [6], showing that the behavior near threshold is determined by non-Coulombic behavior due

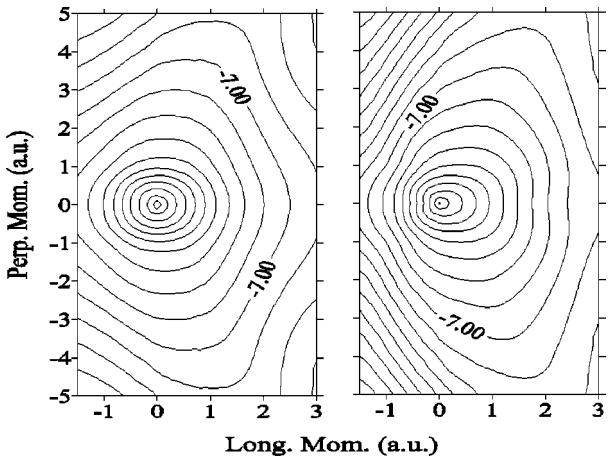

FIG. 6. Same as Fig. 3, but for electron emission from all states of Ar.

to the target potential and a two-center effect due to combined action of the residual target and projectile potentials.

Further insight can be gained by a simple momentum analysis of the collision. In ion-atom collisions at intermediate to high impact energy, the momentum transfer from the projectile is given by $\vec{q}=\vec{\eta}+q_{\parallel}\hat{v}$. The longitudinal momentum transfer is given by $q_{\parallel}=(\frac{1}{2}p_e^2+|\varepsilon_i|)/v$ where ε_i is the initial binding energy. Therefore in the limit of $p_e \ll v$ we have $q_{\parallel}\simeq 0$ and $\vec{q}\simeq\vec{\eta}$, and thus the projectile essentially probes the transverse nodal plane of the initial bound state. This result shows a particular feature of low-energy electron emission. The dependence of the distribution on the initial state appears because in this region the projectile momentum transfer is mainly in the perpendicular direction. As the electron momentum increases, we can expect that these signatures will be lost because the longitudinal momentum transfer washes out this information. It must be noted that in the case of H^+ impact, the processes is closely related to that of electron loss to low-lying continuum states in the projectile field in collisions between atoms. Studies by Bürgdorfer [16] in the case of electron loss from H, initially prepared in the $2p_0$ initial state with Ar targets, showed the same momentum distribution as shown here in Fig. 4. The main difference is that in the case of ionization the projectile is a charged particle, while in the case of electron loss the same role is played by a target which remains neutral throughout the collision. Therefore, in the latter the momentum distribution is not perturbed by the target field, while in the former the charged projectile produces a shift of the distribution in the forward direction.

IV. CONCLUSIONS

In the present work we have shown that OEP's are a valid alternative to HFS potentials, giving cross sections in very good agreement with experiments. These potentials are also free from unphysical results due to the incorrect behavior of the HFS potentials at large distances.

Calculations restricted to very low electron emission energy for given initial states show distinct features which can be related to the nodal structure of the initial bound state. It may be possible to observe such structures in experiments using state-prepared targets.

ACKNOWLEDGMENTS

We acknowledge support from GSI, NSF, DOE, and the Deutsche Forschungsgemeinschaft within the SFB276 and the Leibniz-program. We thank L. Gulyás for providing us with his results shown in Fig. 2. P. D. F. is grateful for the hospitality at the University of Freiburg, and acknowledges fruitful discussions with R. D. Rivarola and support from ANPCyT (Grant No. 03-04021).

[1] N. Stolterfoht, R. DuBois, and R. D. Rivarola, *Electron Emission in Heavy Ion–Atom Collision* (Springer-Verlag, Berlin, 1997).
[2] P.D. Fainstein, V.H. Ponce, and R.D. Rivarola, J. Phys. B **24**, 3091 (1991).
[3] J. Ullrich *et al.*, J. Phys. B **30**, 2917 (1997).
[4] W. Schmitt *et al.*, Phys. Rev. Lett. **81**, 4337 (1998).
[5] R. Moshammer *et al.*, Phys. Rev. Lett. **83**, 4721 (1999).
[6] P.D. Fainstein, L. Gulyás, F. Martín, and A. Salin, Phys. Rev. A **53**, 3243 (1996).
[7] D.H. Madison, Phys. Rev. A **8**, 2449 (1973).
[8] D.S.F. Crothers and J.F. McCann, J. Phys. B **24**, 3091 (1983).
[9] L. Gulyás, P.D. Fainstein, and A. Salin, J. Phys. B **28**, 245 (1995).
[10] F. Herman and S. Skillman, *Atomic Structure Calculations* (Prentice-Hall, Englewood Cliffs, N J, 1963).
[11] L. Gulyás, T. Kirchner, T. Shirai, and M. Horbatsch, Phys. Rev. A **62**, 022702 (2000).
[12] J.D. Talman and W.F. Shadwick, Phys. Rev. A **14**, 36 (1976).
[13] K. Aashamar, T.M. Luke, and J.D. Talman, At. Data Nucl. Data Tables **22**, 443 (1978).
[14] K. Aashamar, T.M. Luke, and J.D. Talman, Phys. Rev. A **19**, 6 (1979).
[15] T. Kirchner, L. Gulyás, H.J. Lüdde, E. Engel, and R.M. Dreizler, Phys. Rev. A **58**, 2063 (1998).
[16] J. Burgdörfer, Phys. Rev. Lett. **51**, 374 (1983).